

# Diffuse stellar emission in X-ray luminous galaxy clusters at $z \sim 0.3$

## I. Is the diffuse optical light boosted and rejuvenated in merging clusters?

D. Pierini<sup>1</sup>, S. Zibetti<sup>2</sup>, F. Braglia<sup>1</sup>, H. Böhringer<sup>1</sup>, A. Finoguenov<sup>1</sup>, P. D. Lynam<sup>3</sup>, and Y.-Y. Zhang<sup>4</sup>

<sup>1</sup> Max-Planck-Institut für extraterrestrische Physik, Giessenbachstrasse, D-85748 Garching bei München, Germany  
e-mail: dpierini, fbraglia, hxb, alexis@mpe.mpg.de

<sup>2</sup> Max-Planck-Institut für Astronomie, Königstuhl 17, D-69117 Heidelberg, Germany  
e-mail: zibetti@mpia-hd.mpg.de

<sup>3</sup> ESO, Karl-Schwarzschild-Strasse 2, D-85748 Garching bei München, Germany  
e-mail: plynam@eso.org

<sup>4</sup> Argelander-Institut für Astronomie, Rheinische Friedrich-Wilhelms-Universität Bonn, Auf dem Hügel 71, D-53121 Bonn, Germany  
e-mail: yyzhang@astro.uni-bonn.de

Received ..., 2008; accepted ...

### ABSTRACT

**Context.** Clusters of galaxies host a diffuse population of intergalactic stars. Diffuse optical light is observed in clusters up to redshift  $z \sim 0.4$ . Recent cosmological hydrodynamical simulations show that this intracluster light originates nearly in parallel with the build-up of the brightest cluster galaxy (BCG), as identified at  $z = 0$ . However, theory proposes alternative scenarios for its origin.

**Aims.** We searched for diffuse stellar emission around BCGs in three of the most X-ray luminous clusters found at  $z \sim 0.3$  in the REFLEX cluster survey and observed with XMM-Newton. These systems (RXCJ 0014.3–3022, RXCJ 0232.2–4420, and RXCJ 2308.3–0211) are in different dynamical states, as witnessed by their X-ray morphology and optical appearance (e.g. multiplicity of BCGs).

**Methods.** Existing medium-deep, wide-field imaging in B and R bands allows extension, intensity, and colour of the stellar emission to be determined across a region that encompasses the X-ray emission from the intracluster medium (ICM) in each cluster.

**Results.** Diffuse stellar emission is robustly detected down to a surface brightness of 26 R-mag arcsec<sup>-2</sup> (observed frame) around a total of seven BCGs, extending up to galactocentric distances of  $\sim 100 h_{70}^{-1}$  kpc. In particular, it surrounds a pair of BCGs in RXCJ 0232.2–4420, while it bridges two BCGs associated with the minor subcomponent of the merging cluster RXCJ 0014.3–3022. The diffuse light detected at the greatest distances from the BCGs of the rather regular clusters RXCJ 0232.2–4420 and RXCJ 2308.3–0211 follows the ICM distribution. Its B – R colour is consistent with the colours measured within the BCG effective radii. The diffuse light around the two pairs of BCGs in RXCJ 0014.3–3022 exhibits bluer colours than the BCG central regions by up to 0.5 mag.

**Conclusions.** If the contribution of the intracluster light (ICL) to the detected diffuse light around BCGs is not negligible, ICL and BCGs have similar stellar populations in relatively relaxed clusters. Merging on a cluster scale eventually adds gravitational stresses to BCGs and other galaxies in subcluster cores. This event may affect the properties of the diffuse stellar emission around BCGs. Shredding of star-forming, low-metallicity dwarf galaxies is favoured as the cause of the bluer B – R colours of the diffuse stellar component around the two pairs of BCGs in the merging cluster RXCJ 0014.3–3022.

**Key words.** X-rays: galaxies: clusters – galaxies: clusters: general – galaxies: elliptical and lenticular, cD – galaxies: evolution – galaxies: interactions – diffuse radiation

## 1. Introduction

A diffuse population of intergalactic stars exists in galaxy clusters, which has been well-established observationally in *individual* systems as well as in a *statistical* sense (see Zibetti 2007 for a review). Observations of this intracluster light (ICL) in individual clusters now extend up to redshifts  $0.3 \lesssim z \lesssim 0.4$  (Krick & Bernstein 2007; Rines et al. 2007). For nearby clusters, the *photometric* detection of the ICL reaches down to very faint surface brightness levels, from  $\sim 26$  down to  $\sim 30$  R-mag arcsec<sup>-2</sup> (Bernstein et al. 1995; Gonzales et al. 2000, 2005; Feldmeier et al. 2002, 2004). Only in a few such systems, however, the presence of intergalactic stars *not* bound to any galaxy could be convincingly proved through a *dynamical* evidence (Arnaboldi et al. 2004). In a complementary approach (Zibetti et al. 2005), stacking images of 683 clusters at  $0.2 \lesssim z \lesssim 0.3$

allowed an average surface brightness of the ICL between  $\sim 26$  and  $\sim 32$  R-mag arcsec<sup>-2</sup> to be reached. This technique made a photometric detection of the ICL possible at much deeper levels, enabling the spatial distribution and colour of the ICL to be studied at extremely large distances (up to  $700 h_{70}^{-1}$  kpc) from the brightest cluster galaxy (BCG). The ICL contributes on average 30–40% to the total optical emission (including galaxies) at  $\sim 100 h_{70}^{-1}$  kpc; this fraction decreases to  $\lesssim 5\%$  at a galactocentric distance of 600–700  $h_{70}^{-1}$  kpc.

On one hand, the radial behaviour of the ICL fraction and the consistency between the optical colours of ICL and BCGs point to an origin of the ICL from galaxies that experience very strong tidal interactions close to the bottom of a cluster’s potential well, and eventually merge into the brightest cluster galaxy (Zibetti et al. 2005). This interpretation is consistent with the kinematic evidence that intracluster planetary nebulae originate

from the ongoing subcluster merger in the Coma cluster core (Gerhard et al. 2007). However, nearby clusters like Virgo exhibit a wealth of tidal structures (e.g. Mihos et al. 2005), which witnesses that stars can be injected all over the cluster environment. The same conclusion is reached in the study of flux, profile, colour, and substructure of the ICL in 10 clusters with different redshifts, X-ray and optical properties (Krick & Bernstein 2007). Consistently, the extent of the ICL and its similar elongation to the cluster galaxy distribution in 24 galaxy clusters at  $0.03 < z < 0.13$  suggest that the evolution of the ICL is tied to the cluster as a whole rather than to the BCG (Gonzalez et al. 2005). However, this correspondence does not always hold (see Feldmeier et al. 2004).

As for the ICL origin, several mechanisms may be at work to some extent, as theory proposes (Sommer-Larsen et al. 2005; Rudick et al. 2006; Murante et al. 2007; Purcell et al. 2007; Conroy et al. 2007). The bulk of the intracluster stars may originate in (proto)galaxies, which have been partly or fully disrupted through tidal stripping in the main cluster potential or by galaxy-galaxy interactions (Sommer-Larsen et al. 2005). Conversely, Murante et al. (2007) show that the formation of the diffuse stellar component in clusters is parallel to the build-up of the brightest cluster galaxy and other massive galaxies, whereas dissolved galaxies contribute only 25% to the ICL budget. Finally, for Purcell et al. (2007), different shredded galaxies are the source of diffuse intrahalo light on varying scales. The diffuse light in group and cluster halos is built from satellite galaxies that form stars efficiently; intracluster light is dominated by material liberated from galaxies with a stellar mass larger than  $\sim 10^{11} M_{\odot}$ .

A significant fraction,  $\sim 30\%$ , of stars needs to be scattered to the diffuse stellar component of clusters at each galaxy-galaxy merging to account for the little evolution of the high end of the stellar mass function of galaxies since  $z \sim 1$ , which turns to be consistent with the total amount of the ICL observed in clusters (Monaco et al. 2006). On the other hand, model brightest cluster galaxies assemble surprisingly late: half of their final mass is typically locked up in a single galaxy after  $z \sim 0.5$  (De Lucia & Blaizot 2007). These two theoretical results prompted our search for diffuse stellar emission around BCGs in the 13 most X-ray luminous clusters at  $z \sim 0.3$  in the ROSAT-ESO Flux-Limited X-ray (REFLEX) cluster survey (Böhringer et al. 2001) and observed with XMM-Newton (Zhang et al. 2006).

Krick & Bernstein (2007) have already detected diffuse light in one of the clusters of our sample (i.e., RXCJ 0014.3–3022 alias AC 118, see Zhang et al. 2004). We confirm their discovery and discuss the properties of the diffuse light around the two pairs of BCGs in this merging system in much greater detail.

Throughout this paper we adopt a  $\Lambda$  cold dark matter (CDM) cosmological model where  $\Omega_m = 0.3$ ,  $\Omega_{\Lambda} = 0.7$ , and  $H_0 = 70 h_{70} \text{ km s}^{-1} \text{ Mpc}^{-1}$ , which is consistent with the main results of Spergel et al. (2007). Hence a metric separation of 1 Mpc corresponds to an angular distance of 3.75 arcmin at  $z = 0.3$ .

## 2. The sample

For this pilot study, we selected three objects from the REFLEX Distant X-ray Luminous (DXL) cluster sample (Zhang et al. 2006) with existing optical imaging. Table 1 lists denomination, redshift, characteristic radius  $R_{500}^1$ , X-ray bolometric luminosity and classification of each cluster (from Zhang et al. 2006).

<sup>1</sup>  $R_{500}$  is the radius within which the average density of the DM in the cluster is 500 times the critical density of the Universe.

In spite of its small size, our sample spans the range in X-ray morphology (or the dynamical state of a cluster, see Jones & Forman 1992) of the most X-ray luminous clusters at  $z \sim 0.3$ . It complements the sample of Krick & Bernstein (2007), which spans a range in cluster characteristics, namely redshift ( $0.05 \lesssim z \lesssim 0.3$ ), morphology (i.e., number of BCGs), spatial projected density (richness class 0–3), and X-ray luminosity ( $1.9 \times 10^{44} \text{ erg s}^{-1} < L_X < 22 \times 10^{44} \text{ erg s}^{-1}$  for the cosmology adopted here). As the latter sample, ours is X-ray selected whereas that of Zibetti et al. (2005) was originally selected in the optical with a maxBGC method (Koester et al. 2007a, 2007b).

## 3. Observations

The selected objects were observed with XMM-Newton in AO-1 and AO-3 as part of the REFLEX-DXL cluster sample (Zhang et al. 2006). All pointed observations were performed with thin filter for the three detectors of the European Photon Imaging Camera (EPIC) on XMM-Newton (Strüder et al. 2001; Turner et al. 2001). The MOS data were taken in Full Frame (FF) mode, whereas the *pn* data were taken in Extended Full Frame (EFF) mode in AO-1 and FF mode in AO-3. For *pn*, the fractions of the out-of-time (OOT) effect are 2.32% and 6.30% for the EFF mode and FF mode, respectively. An OOT event file is created and used to statistically remove the OOT effect. Total exposure times were equal to 18.3 ks, 13.6 ks, and 11.9 ks for RXCJ 0014.3–3022, RXCJ 0232.2–4420, and RXCJ 2308.3–0211, respectively.

The same clusters were observed with the Wide Field Imager (WFI, Baade et al. 1999) mounted at the Cassegrain focus of the ESO/MPG 2.2m telescope in La Silla, Chile (Pierini et al., in preparation). This is a  $4 \times 2$  mosaic detector of  $2k \times 4k$  CCDs with pixel scale of  $0.238''/\text{pixel}$ , which gives a field of view per exposure of  $34' \times 33'$ . Data were taken in the B ( $\lambda_0 = 4562.52 \text{ \AA}$ ), V ( $\lambda_0 = 5395.62 \text{ \AA}$ ), and R<sub>c</sub> ( $\lambda_0 = 6517.25 \text{ \AA}$ , hereafter simply R) bands. In particular the B and R broad-band filters nicely probe the spectral region across the  $4000 \text{ \AA}$  break, which sets some constraints on the characteristics of the bulk of stellar populations existing at  $z \sim 0.3$  (see Fig. 10). So only B and R imaging is used in this study. Observations were performed on September 27–30, 2000 under photometric conditions and with a seeing of  $1.0\text{--}1.3''$  (FWHM). They were not aimed at detecting diffuse light but at characterising clusters (see Böhringer et al. 2006). Total exposure times were equal to 4800 s (B), 3600 s (V), and 3600 s (R), i.e., 6 times shorter than the average total exposure times in V and r bands of the data collected by Krick & Bernstein (2007) at the 2.5m du Pont telescope for their two galaxy clusters at  $z = 0.3$  (i.e., AC 114 and AC 118). Twilight-sky flats were taken in the evening and following morning for each night of observations. A dithering pattern with dithers up to a few arcmin was applied between individual exposures (eight per filter). This reduces large-scale flat-fielding fluctuations on combination. However, our WFI data prevent a detection of diffuse light down to the surface brightness levels reached by Krick & Bernstein (2007) through their optimized observing strategy.

## 4. Analysis

Figs. 1–3 reproduce the X-ray surface brightness distribution in a square region of 2.0 Mpc on a side next to the corresponding R-band image for the individual clusters. The X-ray map represents the projected distribution of gas at temperatures of  $10^7\text{--}10^8 \text{ K}$ , which makes the bulk of the intracluster medium (ICM). A total of seven BCGs can be clearly identified on the R-band images, whose basic properties are listed in Table 2.

Details of the EPIC X-ray data reduction, analysis, and results are described in Zhang et al. (2006). For the WFI optical data, we made use of the data reduction system developed for the ESO Imaging Survey (EIS, Renzini & da Costa 1997) and its associated EIS/MVM image processing library version 1.0.1 (*Alambic*, Vandame 2004). The B- and R-band combined images of each cluster were registered and matched to the same seeing. Magnitudes were calibrated to the Johnson–Cousins filter system using ancillary observations of standard star fields (Landolt 1992). They were corrected for atmospheric extinction and galactic extinction (Schlegel et al. 1998). They are expressed in the Vega system hereafter. The photometric quality reached by the optical images is such that the background RMS on the pixel scale of the R-band images (the deepest ones) corresponds to 25.74, 25.81, and 25.38 R-mag arcsec<sup>-2</sup> for RXCJ 0014.3–3022, RXCJ 0232.2–4420, and RXCJ 2308.3–0211, respectively. For the same images, the  $1\sigma$  background fluctuations amount, respectively, to 28.25, 27.51, and 27.15 R-mag arcsec<sup>-2</sup>, as measured in 100-pixels wide annuli with inner radius corresponding to  $R_{500}$  centred on each BCG. Scales of 100 pixels are relevant to the measurement of the diffuse light.

#### 4.1. Notes on individual clusters

##### 4.1.1. RXCJ 0014.3–3022

The complex X-ray aspect and galaxy distribution witness an ongoing cluster merging. Two visual pairs of BCGs,  $\sim 740$  kpc apart (projected distance), can be easily identified in Fig. 1. The photometric redshifts of the individual BCGs are consistent with those of their parent substructures (from Braglia et al. 2007). The two X-ray subcomponents of the system are displaced from their corresponding pairs of BCGs by  $\sim 210$  kpc. Comparison of X-ray aspect and galaxy distribution between RXCJ 0014.3–3022 and the famous “Bullet Cluster” (see Clowe et al. 2006) suggests that the former is at an earlier stage of merging, when the less massive DM subcomponent is still falling in towards the most massive one. This is consistent with the conclusion from the substructure analysis of RXCJ 0014.3–3022 by Braglia et al. (2007).

One visual pair of BCGs lies to the north-west with respect to the X-ray centroid (i.e., RXCJ 0014.3–3022NW A and B). The projected separation of the two BCGs is  $\sim 185$  kpc. Lack of spectroscopy for RXCJ 0014.3–3022NW B does not permit the physical nature of the pair to be established, but RXCJ 0014.3–3022NW is associated with an X-ray feature connecting the two subcomponents of the ICM. At the angular resolution of XMM-Newton (6" FWHM), there is no evidence that this X-ray bridge results from the superposition of two weak point-like sources (i.e., X-ray emitting active galactic nuclei). The conclusion that this extended X-ray structure is made of hot gas still confined in the potential well of RXCJ 0014.3–3022NW, in spite of the ongoing large-scale merging, is tantalizing<sup>2</sup>. The second visual pair of BCGs, to the south-east, (i.e., RXCJ 0014.3–3022SE A and B) is actually made of two very close pairs of galaxies at consistent photometric redshifts. A main component (i.e., one of the two BCGs) can be clearly identified in each of these very close pairs (see also Fig. 5). The two BCGs are separated by  $\sim 120$  kpc on the plane of the sky and by  $4119 \pm 416$  km s<sup>-1</sup> (rest frame) along the line of sight (from Braglia et al. 2007). Hence, likely

<sup>2</sup> For recent N-body/SPH simulations of interacting clusters see Mastropietro & Burkert (2007).

RXCJ 0014.3–3022SE is not an interacting pair. Its environment can be thought as analogous to the inner region of the richness 2 cluster A 3888 at  $z = 0.15$  (Krick et al. 2006).

##### 4.1.2. RXCJ 0232.2–4420

The distribution of the X-ray emission is not centrally symmetric (note the broad extension to the south-west in Fig. 2), meaning that this cluster is not fully relaxed. A small, secondary, extended X-ray source is found in the ESE direction. It is apparently disconnected from the primary X-ray emission component (i.e., RXCJ 0232.2–4420) at the sensitivity limit reached by the XMM-Newton observations. In the cluster core sits a visual pair of BCGs, separated by  $\sim 100$  kpc on the plane of the sky. One (i.e., RXCJ 0232.2–4420 A, see Table 2) coincides with the X-ray peak and centroid.

##### 4.1.3. RXCJ 2308.3–0211

The distribution of the X-ray emission is centrally symmetric. A single BCG is at the centre of this fairly regular cluster.

#### 4.2. Detection of a diffuse stellar component

The upper panels of Figs. 4–7 show zoom-in’s of the R-band images of the clusters, centred on their (pairs of) BCGs. Isophotal contours are drawn down to 26 mag arcsec<sup>-2</sup>; they clearly show diffuse luminous envelopes around all seven BCGs. Diffuse stellar emission is detected down to 26 R-mag arcsec<sup>-2</sup> not only around the BCGs but also around other bright member galaxies, as in RXCJ 0014.3–3022<sup>3</sup>. However, we keep our focus on the core regions of galaxy clusters and refer the reader to Krick & Bernstein (2007) for a discussion of the ICL forming earlier in infalling groups and later combining in the cluster centre.

The surface brightness distribution of the seven BCGs is further analysed by means of elliptical isophote fitting (through the IRAF<sup>4</sup> task `ellipse`) and azimuthally averaged surface brightness profiles. This is reported in Fig. 8, where data points are logarithmically spaced. Other galaxies are conservatively masked out before elliptical isophotes are fitted. We take a similar approach as Seigar et al. (2007) and decompose each profile in two components: an inner “de Vaucouleurs”  $r^{1/4}$ -law (de Vaucouleurs 1948) and an external exponential component. The only exception is the BCG of RXCJ 2308.3–0211, for which a double exponential represents a better fit. Fits are performed assigning the same weight to each data point in order to properly weigh the outer parts of the profiles. These would be highly under-weighted in a scheme based on the signal-to-noise ratio (S/N). Furthermore, points at semi-major axis smaller than the seeing FWHM are excluded. We stress, however, that the actual analytic model or weighting scheme adopted is not crucial for the qualitative arguments discussed below.

For five out of seven BCGs (i.e., RXCJ 0014.3–3022NW A and B, RXCJ 0014.3–3022SE A, and RXCJ 0232.2–4420 A and B), the best-fit decomposition is given by an inner “de Vaucouleurs” plus a very flat outer exponential. This is suggestive of a “classical” elliptical core living in a very diffuse

<sup>3</sup> Membership can be assigned from the spectroscopic and/or photometric redshifts determined in Braglia et al. (2007).

<sup>4</sup> IRAF is distributed by the National Optical Astronomy Observatories, which are operated by the Association of Universities for Research in Astronomy, Inc., under cooperative agreement with the National Science Foundation.

halo with  $\mu_R \gtrsim 25$  mag arcsec $^{-2}$  (cf. e.g. Schombert 1987). A single ‘‘Sérsic’’ profile (Sérsic 1968) provides a much worse fit in all these five cases. For the other two BCGs, the inner profile is more complex than a single ‘‘de Vaucouleurs’’ law and the contamination by nearby galaxies does not enable us to extend the profile as deep as to reach the alleged surface brightness limit where the diffuse component takes over. We note that these results are in reasonable agreement with those of Seigar et al. (2007), based on a sample of five nearby cDs.

As the faintest R-band isophotes drawn in Figs. 4–7 indicate, the detected diffuse stellar emission extends up to  $\sim 100$  kpc from the (closest) BCG. This extent is well beyond the (projected) R-band effective radius of individual BCGs, which measures  $\sim 7.5$ – $27.4$  kpc (see  $r_{e,R}$  in Table 2). This gives us confidence that a non-negligible fraction of the light detected at the largest distances from the individual BCGs is emitted by stars that are free-floating in the cluster rather than gravitationally bound to a BCG. As a comparison, Zibetti et al. (2005) find that on average 30–40% of the emission detected at such large distances is due to the intracluster component.

The detection of diffuse light in our images is robust in spite of their relatively short exposures (cf. Krick & Bernstein 2007). In fact, the 26 R-mag arcsec $^{-2}$  isophotes drawn in Figs. 4–7 are significant at the 3– $5.7\sigma$  level by assuming that background fluctuations represent the main source of uncertainty. As a further proof of the reliability of our detections, we confirm the presence of diffuse stellar emission in RXCJ 0014.3–3022 at the same locations where it was discovered by Krick & Bernstein (2007).

#### 4.3. Diffuse stellar emission and intracluster medium

If a relevant fraction of the diffuse stellar emission around BCGs is not bound to any BCG, the projected distribution of this component can be expected to deviate from the isophotal shape of the BCG(s) and resemble the projected distribution of the cluster’s DM halo. This is mapped by the X-ray emitting gas in relatively relaxed clusters (e.g. Allen et al. 2002).

The distribution of the diffuse light around the pair of BCGs in RXCJ 0232.2–4420 resembles that of the envelopping X-ray emitting gas. The centres of these two BCGs are aligned in the EW direction and separated by  $\sim 100$  kpc; the major axes of RXCJ 0232.2–4420 A and B have position angles (measured counter-clockwise from north to east) of about  $45^\circ$  and  $100^\circ$ , respectively (see Fig. 6). The cocoon of diffuse stellar emission within the 26 R-mag arcsec $^{-2}$  isophote exhibits a SW extension which reaches out to  $\sim 80$  kpc towards the west at a galactocentric distance of  $\sim 90$  kpc along the direction of the major axis of RXCJ 0232.2–4420 A. This behaviour is analogous to that of the X-ray emission of the cluster, whose projected distribution is centred on RXCJ 0232.2–4420 A but deviates from centrally symmetry owing to a broad SW extension (see Fig. 2).

RXCJ 2308.3–0211 exhibits some correspondence between the distributions of diffuse light and X-ray emission (see Fig. 3). In this fairly regular cluster, there is a single BCG and the X-ray emission peak coincides with its position. Thus, an alignment between the major axes of the BCG and the potential well of its parent cluster could be expected (Brown 1997; Dubinski 1998 and references therein). The ‘‘peculiar’’ R-band radial surface brightness profile of the BCG in RXCJ 2308.3–0211 (see Fig. 8) may witness the presence of diffuse light not bound to the BCG.

The ICM does not necessarily trace DM in a merging cluster like RXCJ 0014.3–3022 (cf. Clowe et al. 2006). There diffuse light is detected around two pairs of BCGs, which probably ex-

perience severe gravitational stresses also owing to the ongoing large-scale merging. In particular, RXCJ 0014.3–3022NW suggests strong tidal forces in action: a stellar ‘‘plume’’ stretches out of RXCJ 0014.3–3022NW B along the bridge of diffuse emission connecting the two BCG main bodies - as defined by their effective radii - (see Fig. 4). In absence of spectroscopic evidence of interaction, the stellar plume stretching out of RXCJ 0014.3–3022NW B and the twisted outer isophotes of RXCJ 0014.3–3022NW A support the hypothesis that the stellar bridge between these BCGs is not a projection effect.

#### 4.4. Colour of the diffuse stellar emission around BCGs

Disentangling the contributions of the ICL and BCG to the observed diffuse stellar emission around a BCG can be hampered by galaxy crowding in a cluster core (see Krick & Bernstein 2007 for RXCJ 0014.3–3022). However, a colour analysis may constrain the properties of intracluster stars if the ICL makes on average 30–40% of the total optical emission (including galaxies) at  $\sim 100$  kpc (Zibetti et al. 2005). Therefore, we produce colour maps of our fields and investigate whether the expected presence of intracluster stars of as-yet unknown origin and amount affects the colours of the diffuse light around our sample BCGs. First we adaptively median smooth the images, in both R and B bands. The intensity of each pixel is replaced with the median intensity in a circle whose radius is grown until a minimum S/N is reached. Given the properties of our imaging, we require a minimum S/N of 20 in R, and of 5 in B. The same smoothing is applied in both bands; it results in B – R colour uncertainties smaller than 0.25 mag on all regions with R-band surface brightness  $\mu_R \lesssim 26$  mag arcsec $^{-2}$ . This scheme preserves the full original spatial information and resolution in the highest S/N regions (i.e., within the ‘‘classical’’ optical extent of a galaxy). It also allows optimal S/N measurements of surface brightness and colour to be obtained in low surface brightness regions, such as galaxy outskirts and intergalactic regions. B – R colour maps are obtained from the adaptively median-smoothed images; they are shown in the bottom panels of Figs. 4–7.

Given the nature of the diffuse light and the depth of our photometry, a statistics of the B – R colour of the diffuse stellar emission around BCGs is computed in 20 regions, each of 4.6 square arcsec (i.e.,  $9 \times 9$  square pixels), on individual colour maps. Ten of these regions are located all around each (pair of) BCG(s) but close to the 26 R-mag arcsec $^{-2}$  isophote; 10 are located at a projected distance larger than 50 kpc from the centre of the (closest) BCG. The 20 areas avoid high-surface brightness regions that are clearly associated with other galaxies than the BCGs. They can partially overlap, especially those at the largest distances from the (closest) BCG. In this approach, we consider as the characteristic B – R colour of the diffuse light around each (pair of) BCG(s) the median of the 20 values of the median B – R colour estimated in the different peripheral regions of each (pair of) BCG(s). This choice is motivated by the absence of colour gradients at large distances from the (closest) BCG (see Fig. 9). It also minimizes the impact of contaminating emission at low surface brightness from bright galaxies other than the BCGs, galaxies with very low-surface brightnesses or faint, unresolved sources. For BCGs, total colours  $(B - R)_{\text{tot}}$  are computed from the B and R magnitudes listed in Table 2, whose accuracy mostly depends on source deblending (see Figs. 4–7). In addition, we determine radial B – R colour profiles for the individual BCGs. Elliptical annuli are defined from the R-band elliptical isophotes (Sect. 4.2), whereas average B – R colours inside annular regions are derived from the colour maps. Figure 9

reproduces the  $B - R$  colour of the diffuse light - as measured in individual regions at distances larger than 30 kpc from the centre of the (closest) BCG - (squares) and the  $B - R$  colour profile of the associated BCG(s) (circles) for each (pair of) BCG(s). No  $k$ - nor evolutionary correction is applied to our photometry: they critically depend on the assumption made on the spectral energy distributions of the stellar populations, whose nature is a priori unknown.

In all the seven BCGs the  $B - R$  colour is equal to  $\sim 2.3$ – $2.6$  mag in the central region and becomes bluer at the effective radius, on average by  $\sim 0.2$  mag (see Table 3). This is consistent with observations of the local Universe: colours are remarkably constant within the inner regions of BCGs (Postman & Lauer 1995), and strong colour gradients are on average absent in cD galaxies (e.g., Schombert 1988; Mackie 1992; see however Brown 1997). In the rather relaxed clusters RXCJ 0232.2–4420 and RXCJ 2308.3–0211 the diffuse light around BCGs exhibits the same colour,  $B - R \sim 2.4$ , which is consistent at the  $1$ – $2\sigma$  level with the colours measured within the effective radii of the individual BCGs. Conversely, in the merging cluster RXCJ 0014.3–3022 the diffuse stellar emission around each (pair of) BCG(s) exhibits  $B - R \sim 1.9$ , which is  $0.35 \pm 0.12$  mag bluer than the average total colour  $B - R \sim 2.3$  of the four BCGs, and, a fortiori, of their central regions<sup>5</sup>. The colour profile of one BCG in each pair (i.e., RXCJ 0014.3–3022 NW B and RXCJ 0014.3–3022 SE A) extends out to at least 65 kpc, where its value is consistent with the colour of the diffuse light further out.

## 5. Discussion

The existence of a diffuse population of intergalactic stars in galaxy clusters originating the ICL is well-established observationally, but several interpretations of the ICL are possible (see Sect. 1). In particular, there are observations and simulations which indicate that the formation of the diffuse stellar component around a BCG is mostly associated with the build-up of the BCG itself (Zibetti et al. 2005; Murante et al. 2007). The present understanding of the hierarchical formation of BCGs (De Lucia & Blaizot 2007) foresees that their stars are formed very early (50% at  $z \sim 5$ , 80% at  $z \sim 3$ ) and in many small galaxies. Model BCGs assemble surprisingly late: half their final mass is typically locked up in a single galaxy after  $z \sim 0.5$ . These late mergers do not change the apparent age of BCGs, since they involve the accumulation of a large number of old stellar populations from galaxies with little gas content and red colours. This yields the observed homogeneity of BCG properties in the local Universe (e.g., Schombert 1988; Mackie 1992; Postman & Lauer 1995; von der Linden et al. 2007; see however Brown 1997).

Different observational results from samples of clusters at different redshifts do not lead to a unanimous consensus on this theoretical scenario. For instance, the K-band Hubble diagram for 25 BCGs at  $0 < z < 1$  suggests that the stellar mass in a typical BCG has grown in good agreement with the predictions of semi-analytic models of galaxy formation and evolution set in the context of a hierarchical scenario for structure formation (Aragon-Salamanca et al. 1998). On the other hand, the lack of evidence for evolution of the central-galaxy luminosity–host-halo mass relation for a sample of known BCGs at  $0.1 < z < 0.8$

points to a BCG growth that is still limited by the timescale for dynamical friction at these earlier times, not proceeding according to the predictions of current semi-analytic models (Brough et al. 2008).

Observations of BCGs at intermediate redshifts are crucial for establishing the late assembly of BCGs and understanding the origin of the ICL. Thus, we selected three clusters from the REFLEX-DXL sample (Zhang et al. 2006) with available wide-field optical imaging (Pierini et al. in preparation), i.e.: RXCJ 0014.3–3022, RXCJ 0232.2–4420, and RXCJ 2308.3–0211. This sample is limited but spans the range of dynamical states of the most X-ray luminous clusters at  $z \sim 0.3$ . We cannot tackle important issues such as the evolution of the ICL fraction and colours (see Zibetti et al. 2005; Krick & Bernstein 2007) for lack of statistics and redshift coverage. However, we demonstrate that medium–deep (down to a completeness limit of  $R \sim 23.5$ ), multi-band (B and R bands here) photometry at a 2m-class telescope can foster the knowledge of the ICL in individual clusters at  $z \sim 0.3$ . In fact, we robustly detect diffuse stellar emission down to 26 R-mag arcsec<sup>-2</sup> (observed frame) with 1 hr-exposures. The depth of our photometry enables us to investigate distribution and colour of the diffuse light around BCGs as a function of the dynamical state of a galaxy cluster.

Diffuse stellar emission is detected around all the seven BCGs in the three clusters, and around other bright galaxies in RXCJ 0014.3–3022 (cf. Krick & Bernstein 2007). This diffuse light exceeds the emission from stars with a projected distribution following a  $r^{1/4}$ -law, and extends up to  $\sim 100$  kpc from the centre of the (closest) BCG. At this distance, we expect that on average 30–40% of the diffuse stellar emission is due to the ICL, as from the statistical results obtained from 683 clusters of galaxies at  $0.2 \lesssim z \lesssim 0.3$  (Zibetti et al. 2005). Consistently, the distribution of the diffuse light around BCGs follows the larger-scale distribution of the ICM in a system which is either relaxed (i.e., RXCJ 2308.3–0211) or close to relaxation (i.e., RXCJ 0232.2–4420). There the ICM is expected to trace the DM component, which dominates the mass budget of a cluster. In absence of dynamical information, this is indirect evidence that part of the diffuse stellar emission around three out of seven BCGs is associated with the potential well of their parent clusters.

Comparison of Figs. 1–3 suggests that BCGs and diffuse light around them have distinct dynamical evolutions. This is in agreement with the conclusion of Krick & Bernstein (2007). The diffuse light around the two pairs of BCGs in RXCJ 0014.3–3022 *can be at least in part the result of severe gravitational stresses potentially experienced by these BCGs* (see Sect. 4.3). Each pair of BCGs, offset by  $\sim 210$  kpc from the closest X-ray subcomponent of this merging cluster, probably signposts the minimum of the potential well of each dark matter subcomponent (cf. Clowe et al. 2006). The presence of a pair of BCGs at the centre of RXCJ 0232.2–4420 together with the X-ray morphology (Fig. 2) suggest that this system is evolving towards relaxation, like Coma. The diffuse stellar emission detected at the largest distances from this pair of BCGs follows the distribution of the dark matter (i.e., the X-ray emitting, hot gas), *whether the intergalactic stars were stripped from the BCGs or had a different origin* (see Krick & Bernstein 2007). One can imagine that, later on, the two BCGs will merge into a new dominant galaxy (e.g., Naab et al. 2006; De Lucia & Blaizot 2007), which will sit at the centre of the cluster potential well, and possibly respond to its triaxial configuration. Eventually the cluster will look like RXCJ 2308.3–0211, where the distribution of the diffuse light around the single BCG in the cluster core is aligned

<sup>5</sup> Krick & Bernstein (2007) estimate the colour of the diffuse light in RXCJ 0014.3–3022 to be  $V - r \approx 1.0 \pm 0.8$ , which is significantly redder (0.6 mag) than the cluster red sequence that they determine. Clearly our result is at odds with theirs.

with the major axes of the BCG and of the larger-scale distribution of the ICM (i.e., the dark matter).

All seven BCGs exhibit  $B - R$  colours which differ by up to 0.3 mag in their central regions. A similar narrow spread exists among their colour gradients, when  $B - R$  colours are measured in the central region and at the effective radius of each BCG (see Table 3). These results are consistent with others in the literature (e.g., Schombert 1988; Mackie 1992; Postman & Lauer 1995). They confirm that star formation has occurred over a short time-scale in the BCGs under study (cf. von der Linden et al. 2007 and Bildfell et al. 2008). Furthermore, the  $B - R$  colour of the diffuse light around the BCGs in RXCJ 0232.2–4420 and RXCJ 2308.3–0211 is about as red as the light within the effective radii of the BCGs (see Fig. 9), whether there is a pair of BCGs or a single BCG in the cluster core<sup>6</sup>. This is consistent with the result of Zibetti et al. (2005). Conversely, the  $B - R$  colour of the diffuse light detected around the two pairs of BCGs in RXCJ 0014.3–3022 is bluer than the average colour of the central regions of the two pairs of BCGs by  $0.44 \pm 0.15 - 0.51 \pm 0.20$  mag.

In analogy with early-type galaxies at different redshifts (Saglia et al. 2000; Tamura et al. 2000), mild colour gradients can imply mild metallicity gradients in our BCGs. We make use of the stellar population evolutionary synthesis models in Bruzual & Charlot (2003) to interpret the observed  $B - R$  colours of BCGs and diffuse light. Comparison between Fig. 9 and Fig. 10 shows that the colours measured in the central regions of all the seven BCGs can be reproduced by simple stellar population (SSP) models with at least solar metallicity ( $Z_{\odot}$ ) and age older than 2 Gyr<sup>7</sup>. The colours measured at the effective radius of each BCG can be reproduced with SSP models spanning the same range in age and the range  $\sim 0.4 - 1 \times Z_{\odot}$  in metallicity. Furthermore, the diffuse stellar component around the BCGs in RXCJ 0232.2–4420 and RXCJ 2308.3–0211 has metallicity larger than solar and is probably as old as the central regions of the associated BCG(s). Conversely, the colour of the diffuse light around the two pairs of BCGs in the merging cluster RXCJ 0014.3–3022 can be reproduced with SSP models with age between 0.5 and 4 Gyr and metallicity higher than  $\sim 0.2 \times Z_{\odot}$ . Hence, *there is a difference in the stellar populations responsible for the diffuse light around the BCGs under study.*

The stellar population originating the bluer diffuse light around the two pairs of BCGs in RXCJ 0014.3–3022 can be of internal origin. Under this hypothesis, it is either as old as the stellar populations within the effective radii of the individual BCGs but of lower metallicity, or associated with recent star-formation activity<sup>8</sup>. In the first case, the star formation histories of the four BCGs in RXCJ 0014.3–3022 had to be rather similar, although the two pairs of BCGs inhabited distinguished environments well before the epoch of observation (cf. Sect. 4.1). This can not be excluded on the basis of the available data but is suspicious. On the other hand, in a sample of 48 X-ray luminous galaxy clusters at intermediate redshifts, colour profiles that turn bluer towards their centres are held as evidence for recent star formation in BCGs (e.g., Bildfell et al. 2008). Likely the stars

responsible for the bluer colour of the diffuse light around the two pairs of BCGs in RXCJ 0014.3–3022 were not originated in the BCGs.

This external stellar population may simply be part of unidentified, low surface brightness galaxies that are rather homogeneously distributed around the two pairs of BCGs in RXCJ 0014.3–3022 out to galactocentric distances of  $\sim 100$  kpc (unlikely). If the parent galaxies are faint and unresolved in the WFI images, the FWHM of their R-band surface brightness distribution must be  $\leq 1''$ , which corresponds to  $\leq 4.5$  kpc at  $z \sim 0.31$ . However, imaging of RXCJ 0014.3–3022 SE at comparable depth with respect to the WFI image but at three times-higher angular resolution does not reveal the presence of a significant population of galaxies which are not identified in the latter image (cf. Fig. 11 and Fig. 5). Thus, the bluer colour of the diffuse light in RXCJ 0014.3–3022 may indeed be due to a diffuse stellar component: the intergalactic stars are either produced in situ (unlikely) or come from shredding of galaxies that are bluer than the BCGs (favoured scenario). The longer the duration of the star-formation activity in the galaxies of origin, the lower the mass fraction of these external blue stars (cf. the colours for single burst and continuous star formation models with  $0.2 \times Z_{\odot}$  in Fig. 10). On the other hand, as the mass fraction of the external blue stellar population decreases, younger ages and/or lower metallicities have to be invoked to produce an impact on the observed  $B - R$  colour of the diffuse light.

A clue to the nature of the shredded galaxies is offered by the study of “Butcher–Oemler” clusters (Butcher & Oemler 1978) at  $z = 0.31$  by Couch et al. (1998)<sup>9</sup>, which includes RXCJ 0014.3–3022 (see Fig. 11). These authors concluded that, on average, one in every five cluster members (both blue and red ones) shows morphological signatures indicative of dynamical interactions. Consistently, Fig. 11 shows the presence of several stellar features reminiscent of tails stemming out of galaxies in the neighbourhood of RXCJ 0014.3–3022 SE, as well as a clear asymmetry in the light distribution of RXCJ 0014.3–3022 SE A. Dynamical interactions appear to be a common cause of the most extreme form of star formation activity seen in the clusters investigated by Couch et al. (1998). The galaxies involved are mostly of modest luminosity even in this brightened phase; in their later faded state they appear destined to become dwarfs. For the Sdm/Irr Hubble types among the galaxies with ongoing star formation occurring at the rates typical of normal nearby spirals, their visibility on the HST-WFPC2 images is due mainly to their compact, knotty regions of star formation. These blue, star-forming, dwarf galaxies appear as excellent candidates to explain the bluer  $B - R$  colour of the ICL in RXCJ 0014.3–3022. Once they are shredded, the injected stellar populations would evolve in a passive way - as described by SSPs - and, thus, become redder at  $z = 0$  (cf. Krick & Bernstein 2007). The gravitational stresses tearing them apart could be excited also by the ongoing large-scale merging process, as well as their star formation activity (cf. the case of cluster MS 1054–03 at  $z = 0.83$  in Bai et al. 2007).

Passively evolving, metal poor dwarf galaxies or star-forming giant galaxies with nearly solar metallicities can be alternative candidates according to Fig. 10. Shredding of such galaxies is likely effective also in the non-merging clusters of our sample (e.g., Sommer-Larsen et al. 2005; Purcell et al. 2007; cf. Brown 1997), where the diffuse light is as red as the light within

<sup>6</sup> Isolation and uniqueness of the BCG may have led to the redder core of the dominant central galaxy in RXCJ 2308.3–0211, possibly owing to a lack of recent gas accretions (cf. Bildfell et al. 2008).

<sup>7</sup> The interpretation of broad-band colours suffers from the age-metallicity degeneracy (Worthey 1994).

<sup>8</sup> This holds whether the likely interactions of the two pairs of BCGs in RXCJ 0014.3–3022 were triggered by the large-scale merging or started in the two subcomponents of the system before this event.

<sup>9</sup> The study of star formation rate and morphology by Couch et al. (1998) is based on ground-based spectroscopy plus R (F702W) filter observations with the HST-WFPC2 at a spatial resolution of  $0.3''$ .

the BCG effective radii; it may be enhanced in merging clusters, of course. However, especially if the ICL fraction is lower than average, it is the shredding of metal poor dwarf galaxies with temporarily enhanced star-formation activity the most likely origin of the 0.5 mag-difference in the B – R colour between the diffuse stellar emission around BCGs and the central regions of the BCGs in RXCJ 0014.3–3022.

## 6. Conclusions

We select three clusters of galaxies from the ROSAT-ESO Flux-Limited X-ray (REFLEX) cluster survey: RXCJ 0014.3–3022, RXCJ 0232.2–4420, and RXCJ 2308.3–0211. They span the morphology range of the most X-ray luminous clusters at  $z \sim 0.3$  observed with XMM-Newton (cf. Zhang et al. 2006). Medium-deep, wide-field B- and R-band imaging (Pierini et al. in preparation) allows us to investigate distribution and colour of the diffuse stellar emission around the brightest cluster galaxies (BCGs) as a function of the dynamical state of the parent clusters. This property is inferred from the X-ray morphology and optical appearance (e.g., multiplicity of BCGs) of each cluster.

Diffuse stellar emission is robustly detected around all the seven BCGs in the three X-ray selected clusters, and its distribution and B – R colour down to 26 R-mag arcsec<sup>-2</sup> (observed frame) are investigated. The diffuse light around BCGs extends up to  $\sim 100$  kpc from their centres. At this distance, we expect that on average 30–40% of the detected emission (including galaxies) is due to the intracluster light (ICL), as from the statistical results obtained from 683 optically selected clusters of galaxies at  $0.2 \lesssim z \lesssim 0.3$  (Zibetti et al. 2005).

As a first main result, we find that the distribution of the diffuse stellar emission around BCGs follows the distribution of the intracluster medium (on a larger scale) in a system which is either relaxed, like RXCJ 2308.3–0211, or close to relaxation, like RXCJ 0232.2–4420. In these two cases, the X-ray emitting, hot gas is expected to trace the dark matter fairly well.

In these two X-ray luminous clusters, the B – R colour of the diffuse light around BCGs is as red as the light within the effective radii of the individual BCGs. This holds whether there is a pair of BCGs (in RXCJ 0232.2–4420) or a single BCG (in RXCJ 2308.3–0211) in the cluster core. Hence, we confirm an overall consistency between colours of the ICL and associated BCGs in relatively relaxed galaxy clusters at intermediate redshifts (see Zibetti et al. 2005; Krick & Bernstein 2007). Conversely, we find that the B – R colour of the diffuse stellar emission detected around the two pairs of BCGs in the merging cluster RXCJ 0014.3–3022 is significantly bluer than the central regions of the four BCGs. If the contribution of intracluster stars to the diffuse stellar emission around BCGs is not negligible, this means that the intracluster light has multiple origins, possibly linked to the dynamical state of a cluster.

The B – R colours (observed frame) of the seven BCGs under study and of the diffuse light around the three BCGs in the two X-ray luminous, relatively relaxed clusters RXCJ 0232.2–4420 and RXCJ 2308.3–0211 can be reproduced by simple stellar populations modelled as in Bruzual & Charlot (2003) with at least solar metallicity and age older than 2 Gyr. The diffuse bluer stellar population around the four BCGs in the X-ray luminous, merging cluster RXCJ 0014.3–3022 must have a younger age and/or a lower metallicity than the age and/or metallicity of the characteristic stellar population of the BCGs.

The present picture of the ongoing large-scale merging in RXCJ 0014.3–3022 favours an origin of the bluer diffuse light

detected around its overall “red and dead” BCGs from shredding of star-forming, low-metallicity dwarf galaxies.

*Acknowledgements.* Based on observations made with the ESO/MPG 2.2m telescope at the La Silla Observatory inside the Max Planck Gesellschaft (MPG) time. Based on observations made with the NASA/ESA Hubble Space Telescope, obtained from the data archive at the Space Telescope Science Institute. STScI is operated by the Association of Universities for Research in Astronomy, Inc. under NASA contract NAS 5-26555. D.P. thanks Ortwin Gerhard for a useful discussion regarding this work. D.P. acknowledges support by the German *Deutsches Zentrum für Luft- und Raumfahrt*, DLR project number 50 OR 0405. F.B. acknowledges support by the International Max-Planck Research School (IMPRS) on Astrophysics. H.B. acknowledges support by *The Cluster of Excellence “Origin and Structure of the Universe”*, funded by the Excellence Initiative of the Federal Government of Germany, EXC project number 153.

## References

- Allen, S. W., Schmidt, R. W., & Fabian, A. C. 2002, MNRAS, 334, L11  
Aragon-Salamanca, A., Baugh, C. M., & Kauffmann, G. 1998, MNRAS, 297, 427  
Arnaboldi, M., Gerhard, O., Aguerri, J. A. L., et al. 2004, ApJ, 614, L33  
Baade, D., Meisenheimer, K., Iwert, O., et al. 1999, Msng, 95, 15  
Bai, L., Marcellac, D., Rieke, G. H., et al. 2007, ApJ, 664, 181  
Bernstein, G. M., Nichol, R. C., Tyson, J. A., Ulmer, M. P., & Wittman, D. 1995, AJ, 110, 1507  
Bertin, E., & Arnouts, S. 1996, A&AS, 117, 393  
Bildfell, C., Hoekstra, H., Babul, A., & Mahdavi, A. 2008, arXiv:0802.2712  
Böhlinger, H., Schuecker, P., Guzzo, L., et al. 2001, A&A, 369, 826  
Böhlinger, H., Schuecker, P., Guzzo, L., et al. 2004, A&A, 425, 367  
Böhlinger, H., Braglia, F., Pierini, D., et al. 2006, Msng, 123, 49  
Braglia, F., Pierini, D., & Böhlinger, H. 2007, A&A, 470, 425  
Brough, S., Couch, W., Collins, C., et al. 2008, arXiv:0801.1170  
Brown, J. P. 1997, PhD thesis, University of Toronto  
Bruzual, G., & Charlot, S. 2003, MNRAS, 344, 1000  
Butcher, H., & Oemler, A. 1978, ApJ, 219, 18  
Chabrier, G. 2003, PASP, 115, 763  
Clowe, D., Bradač, M., Gonzalez, A. H., et al. 2006, ApJ, 648, L109  
Conroy, C., Wechsler, R. H., & Kravtsov, A. V. 2007, ApJ, 668, 826  
Couch, W. J., Barger, A. J., Smail, I., Ellis, R. S., & Sharples, R. M. 1998, ApJ, 497, 188  
De Lucia, G., & Blaizot, J. 2007, MNRAS, 375, 2  
de Vaucouleurs G., 1948, Ann. Astrophys., 11, 247  
Dubinski, J. 1998, ApJ, 502, 141  
Feldmeier, J. J., Mihos, J. C., Morrison, H. L., Rodney, S. A., & Harding, P. 2002, ApJ, 575, 779  
Feldmeier, J. J., Mihos, J. C., Morrison, H. L., et al. 2004, ApJ, 609, 617  
Gerhard, O., Arnaboldi, M., Freeman, K. C., et al. 2007, A&A, 468, 815  
Gonzalez, A. H., Zabludoff, A. I., Zaritsky, D., & Dalcanton, J. J. 2000, ApJ, 536, 561  
Gonzalez, A. H., Zabludoff, A. I., & Zaritsky, D. 2005, ApJ, 618, 195  
Jones, C., & Forman, W. 1992, Imaging the Hot Intra Cluster Medium, in Clusters and Superclusters of Galaxies, ed. A. C. Fabian (Kluwer, Dordrecht), NATO ASI Conf. Ser. 366, 49  
Koester, B. P., McKay, T. A., Annis, J., et al. 2007a, ApJ, 660, 221  
Koester, B. P., McKay, T. A., Annis, J., et al. 2007b, ApJ, 660, 239  
Krick, J. E., & Bernstein, R. A. 2007, AJ, 134, 466  
Krick, J. E., Bernstein, R. A., & Pimblet, K. A. 2006, AJ, 131, 168  
Kron, R. G. 1980, ApJS, 43, 305  
Landolt, A. U. 1992, AJ, 104, 340  
Mackie, G. 1992, ApJ, 400, 65  
Mastropietro, C., & Burkert, A. 2007, arXiv:0711.0967  
Mihos, J. C., Harding, P., Feldmeier, J., & Morrison, H. 2005, ApJ, 631, L41  
Monaco, P., Murante, G., Borgani, S., & Fontanot, F. 2006, ApJ, 652, L89  
Murante, G., Giovalli, M., Gerhard, O., et al. 2007, MNRAS, 377, 2  
Naab, T., Khochfar, S., & Burkert, A. 2006, ApJ, 636, L81  
Poggianti, B. M. 1997, A&AS, 122, 399  
Postman, M., & Lauer, T. R. 1995, ApJ, 440, 28  
Purcell, C. W., Bullock, J. S., & Zentner, A. R. 2007, ApJ, 666, 20  
Renzini, A., & da Costa, L. N. 1997, Msng, 87, 23  
Rines, K., Finn, R., & Vikhlinin, A. 2007, ApJ, 665, L9  
Rudick, C. S., Mihos, J. C., & McBride, C. 2006, ApJ, 648, 936  
Schlegel, D. J., Finkbeiner, D. P., & Davis, M. 1998, ApJ, 500, 525  
Schombert, J. M. 1987, ApJS, 64, 643  
Schombert, J. M. 1988, ApJ, 328, 475  
Seigar, M. S., Graham, A. W., & Jerjen, H. 2007, MNRAS, 378, 1575

- Sérsic, J. L. 1968, Atlas de galaxias australes
- Sommer-Larsen, J., Romeo, A. D., & Portinari, L. 2005, MNRAS, 357, 478
- Spergel, D. N., Bean, R., Doré, O., et al. 2007, ApJS, 170, 377
- Strüder, L., Briel, U., Dennerl, K., et al. 2001, A&A, 365, L18
- Turner, M. J. L., Abbey, A., Arnaud, M., et al. 2001, A&A, 365, L27
- Vandame, B. 2004, Alambic v1.0 User's guide
- von der Linden, A., Best, P. N., Kauffmann, G., & White, S. D. M. 2007, MNRAS, 379, 867
- Worthey, G. 1994, ApJS, 95, 107
- Zhang, Y.-Y., Finoguenov, A., Böhringer, H., et al. 2004, A&A, 413, 49
- Zhang, Y.-Y., Böhringer, H., Finoguenov, A., et al. 2006, A&A, 456, 55
- Zibetti, S. 2007, Statistical Properties of the IntraCluster Light from SDSS Image Stacking, in Dark Galaxies and Lost Baryons, ed. J. I. Davies, & M. J. Disney (Cambridge University Press), IAU Symposium, Volume 244, 176
- Zibetti, S., White, S. D. M., Schneider, D. P., & Brinkmann, J. 2005, MNRAS, 358, 949



**Table 1.** Basic properties of the sample clusters of galaxies.

Denomination	$z^a$	$R_{500}/[\text{Mpc}]$	$L_{\text{bol}}/[10^{44} \text{ erg s}^{-1}]$	Classification
RXCJ 0014.3-3022	0.3066	1.24	$21.2 \pm 1.7$	offset centre
RXCJ 0232.2-4420	0.2836	1.30	$18.9 \pm 1.4$	primary with small secondary
RXCJ 2308.3-0211	0.2966	1.24	$12.0 \pm 1.3$	single

<sup>a</sup> For the optical (i.e., spectroscopic) redshifts see Böhringer et al. (2004).

**Table 2.** Photometric properties of the brightest galaxies in the sample clusters.

Denomination <sup>a</sup>	RA(J2000.0) / [HMS]	Dec(J2000.0) / [DMS]	$r_{e,R}^b/[\text{kpc}]$	$\mu_{e,R}^b/[\text{mag arcsec}^{-2}]$	$R_{\text{tot},R}^c/[\text{mag}]$	$(B - R)_{\text{tot}}^c/[\text{mag}]$
RXCJ 0014.3-3022 NW A	00:14:12.969	-30:22:34.50	16.8	23.38	17.84	2.29
RXCJ 0014.3-3022 NW B	00:14:09.976	-30:22:20.52	27.4	24.06	17.92	2.27
RXCJ 0014.3-3022 SE A <sup>d</sup>	00:14:22.051	-30:24:20.05	22.8	23.93	17.67	2.34
RXCJ 0014.3-3022 SE B <sup>d</sup>	00:14:20.677	-30:24:00.15	19.9	24.16	17.56	2.27
RXCJ 0232.2-4420 A	02:32:18.522	-44:20:47.81	17.6	23.25	17.31	2.17
RXCJ 0232.2-4420 B	02:32:16.364	-44:20:47.95	7.5	21.62	17.30	2.25
RXCJ 2308.3-0211	23:08:22.218	-02:11:31.55	23.1	22.05	17.01	2.28

<sup>a</sup> In a pair of BCGs, the letters “A” and “B” identify the eastern and western components, respectively. No ranking in luminosity is used since total magnitudes are affected by deblending, the cluster cores being very crowded with galaxies (see Figs. 4–7).

<sup>b</sup> R-band effective radii  $r_{e,R}$  and surface brightnesses  $\mu_{e,R}$  refer to the inner “de Vaucouleurs” component of each BCG, except for the BCG of RXCJ 2308.3–0211. For this object, effective parameters are derived from the empirical R-band surface brightness profile (see text).

<sup>c</sup> Total R-band magnitudes and  $B - R$  colours (observed frame) were determined after source photometry extraction with *SExtractor* (Bertin & Arnouts 1996) in a flexible (Kron-like, see Kron 1980) elliptical aperture with a Kron-factor of 2.5.

<sup>d</sup> The pair of BCGs RXCJ 0014.3–3022 SE is actually made of two very close pairs (see Fig. 1). The total magnitudes and colours listed here belong to the two main components of this quadruple system (i.e., the BCGs RXCJ 0014.3–3022 SE A and B), as deblended through *SExtractor*.

**Table 3.** Colours of the cluster brightest galaxies and the diffuse light around them.

Denomination	$(B - R)_0^a/[\text{mag}]$	$(B - R)(r_{e,R})^b/[\text{mag}]$	$\frac{\Delta(B-R)^c}{\Delta \log r}/[\text{mag dex}^{-1}]$	$(B - R)_{\text{disc}}^d/[\text{mag}]$
RXCJ 0014.3-3022 NW A	$2.38 \pm 0.02$	$2.20 \pm 0.14$	$-0.15 \pm 0.12$	$1.94 \pm 0.15$
RXCJ 0014.3-3022 NW B	$2.38 \pm 0.02$	$2.09 \pm 0.16$	$-0.21 \pm 0.12$	$1.94 \pm 0.15$
RXCJ 0014.3-3022 SE A	$2.46 \pm 0.02$	$2.18 \pm 0.16$	$-0.21 \pm 0.12$	$1.93 \pm 0.20$
RXCJ 0014.3-3022 SE B	$2.42 \pm 0.04$	$2.26 \pm 0.11$	$-0.13 \pm 0.09$	$1.93 \pm 0.20$
RXCJ 0232.2-4420 A	$2.36 \pm 0.03$	$2.18 \pm 0.09$	$-0.15 \pm 0.08$	$2.37 \pm 0.18$
RXCJ 0232.2-4420 B	$2.29 \pm 0.01$	$2.27 \pm 0.06$	$-0.02 \pm 0.07$	$2.37 \pm 0.18$
RXCJ 2308.3-0211	$2.59 \pm 0.03$	$2.39 \pm 0.18$	$-0.14 \pm 0.14$	$2.35 \pm 0.14$

<sup>a</sup>  $B - R$  colour measured in the BCG central region (i.e., at a radial distance of about 1 kpc along the major axis).

<sup>b</sup>  $B - R$  colour measured at the BCG effective radius.

<sup>c</sup>  $B - R$  colour gradient measured between the BCG effective radius and central region.

<sup>d</sup>  $B - R$  colour of the diffuse stellar component around each (pair of) BCG(s) - see text.

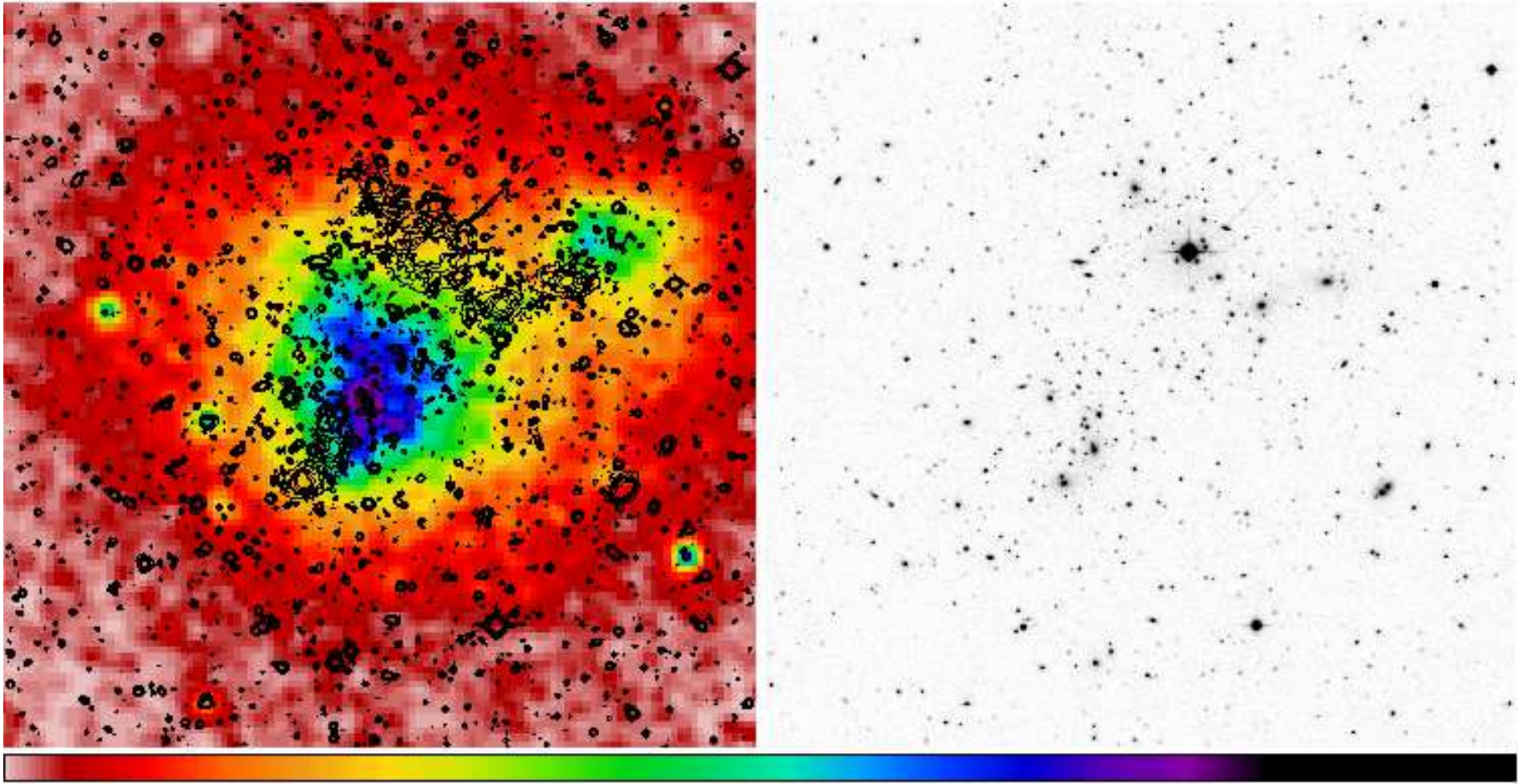


**Fig. 1.** RXCJ 0014.3–3022 as imaged by EPIC (left panel) and WFI (right panel). A square region, 2.0 Mpc on a side, centred on the X-ray centroid of the cluster is reproduced (north is up and east to the left). The X-ray surface brightness distribution is reproduced in a map using a linear scale where intensity increases as the colour moves from the left to the right along the palette at the bottom. An overlay with a black contour map reproduces features in the R-band image at a significance of  $1\sigma$ ,  $2\sigma$ ,  $3\sigma$ ,  $5\sigma$ , and  $10\sigma$ , the limiting surface brightness being equal to  $25.74$  R-mag arcsec $^{-2}$ . The R-band image to the right (in greyscale) highlights high surface brightness regions with a linear scale where intensity increases as the tone turns from light grey to black.

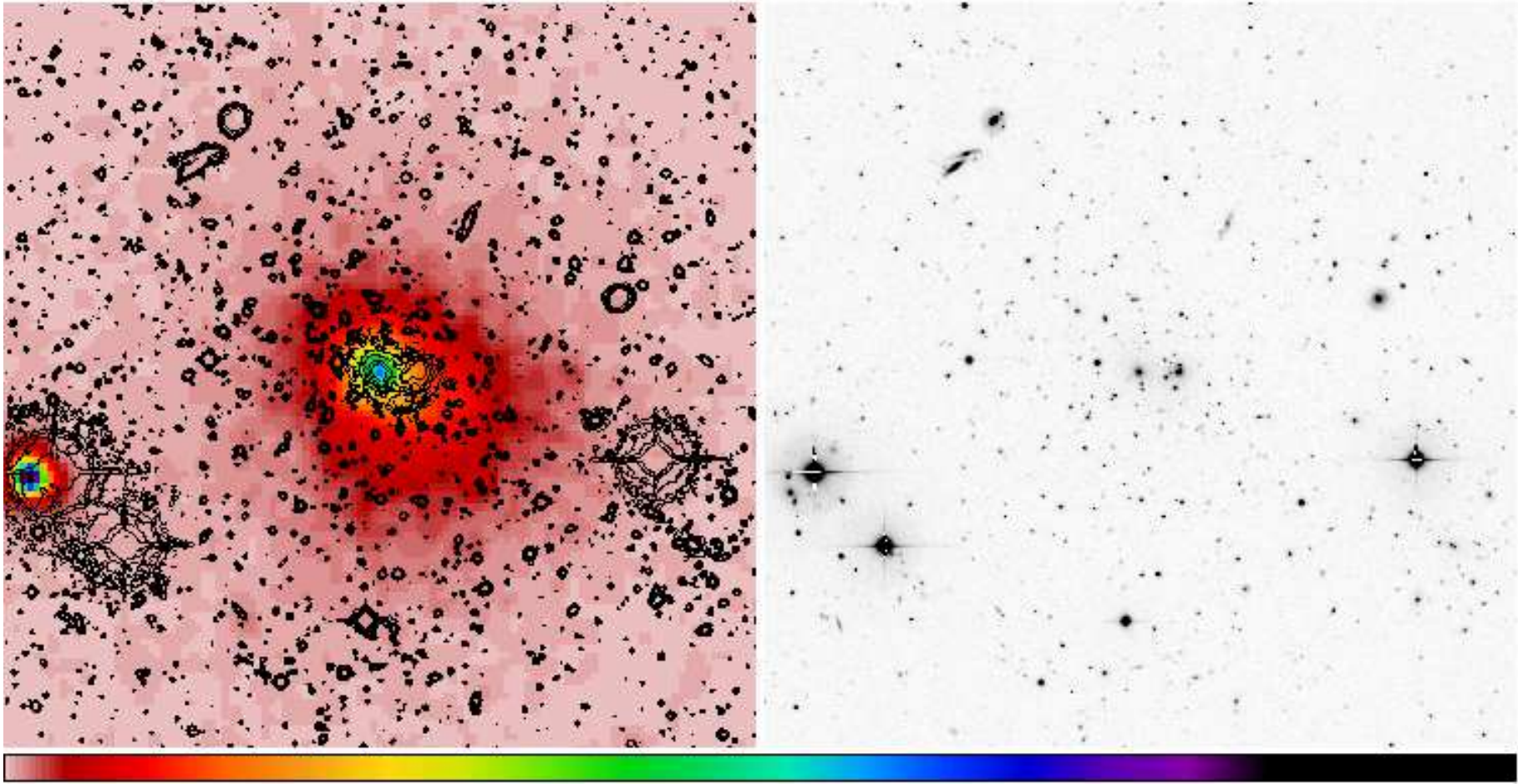


**Fig. 2.** RXCJ 0232.2–4420 as imaged by EPIC and WFI. Size and symbols are the same as in Fig. 1. The limiting R-band surface brightness is equal to  $25.81 \text{ mag arcsec}^{-2}$ . Note the presence of a foreground group of late-type galaxies in the upper half of the R-band image. No detected X-ray emission appears to be associated with this galaxy group.

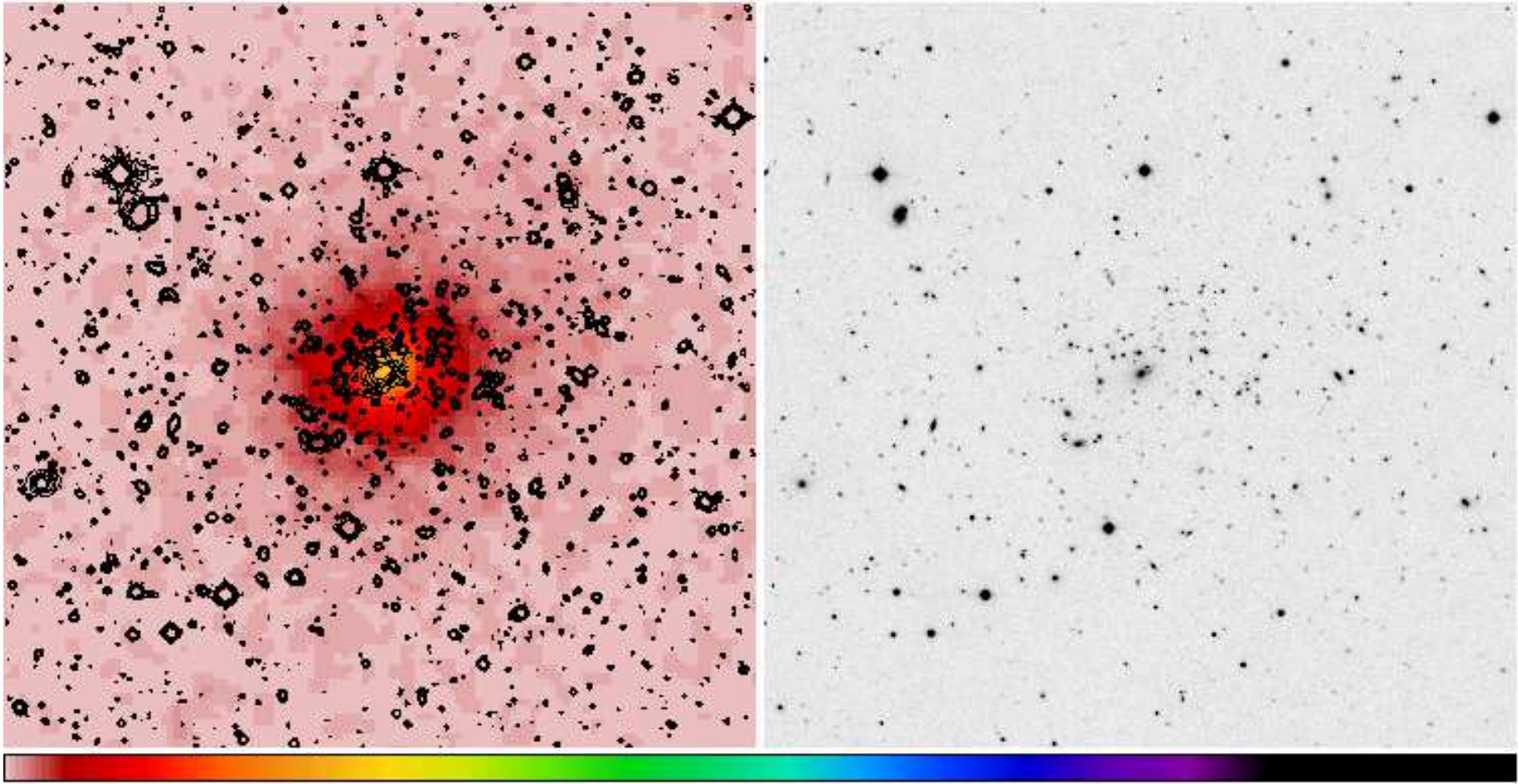


**Fig. 3.** RXCJ 2308.3–0211 as imaged by EPIC and WFI. Size and symbols are the same as in Fig. 1. The limiting R-band surface brightness is equal to  $25.38 \text{ mag arcsec}^{-2}$ .

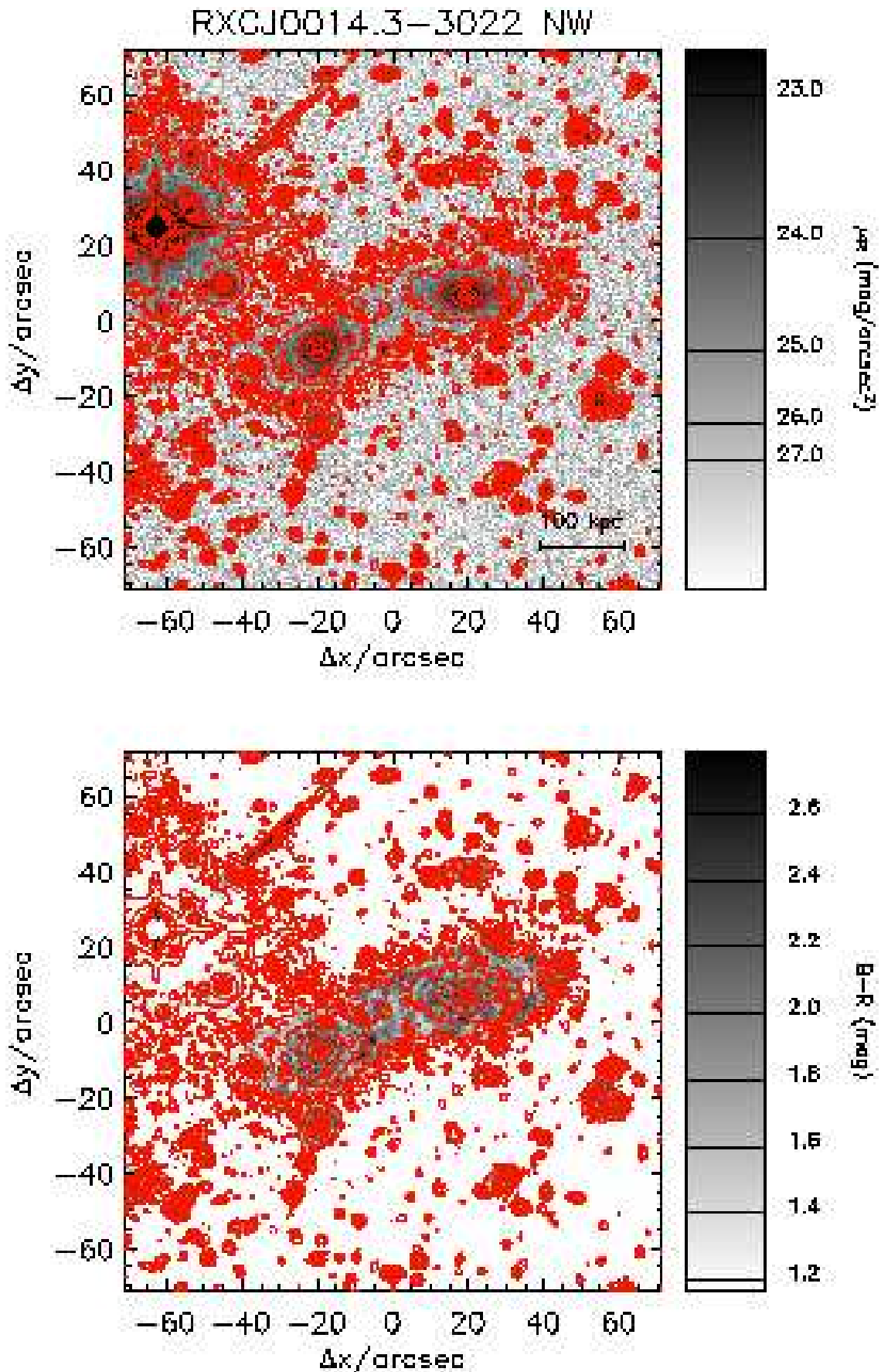


**Fig. 4.** R-band image (top) and adaptively median-smoothed B – R colour (observed frame) map with a limit of 26 R-mag  $\text{arcsec}^{-2}$  (bottom) for RXCJ 0014.3–3022NW. R-band isophotes highlight different objects. Bright galaxies as red as the BCGs are at  $z \sim 0.3$  (Braglia et al. 2007).

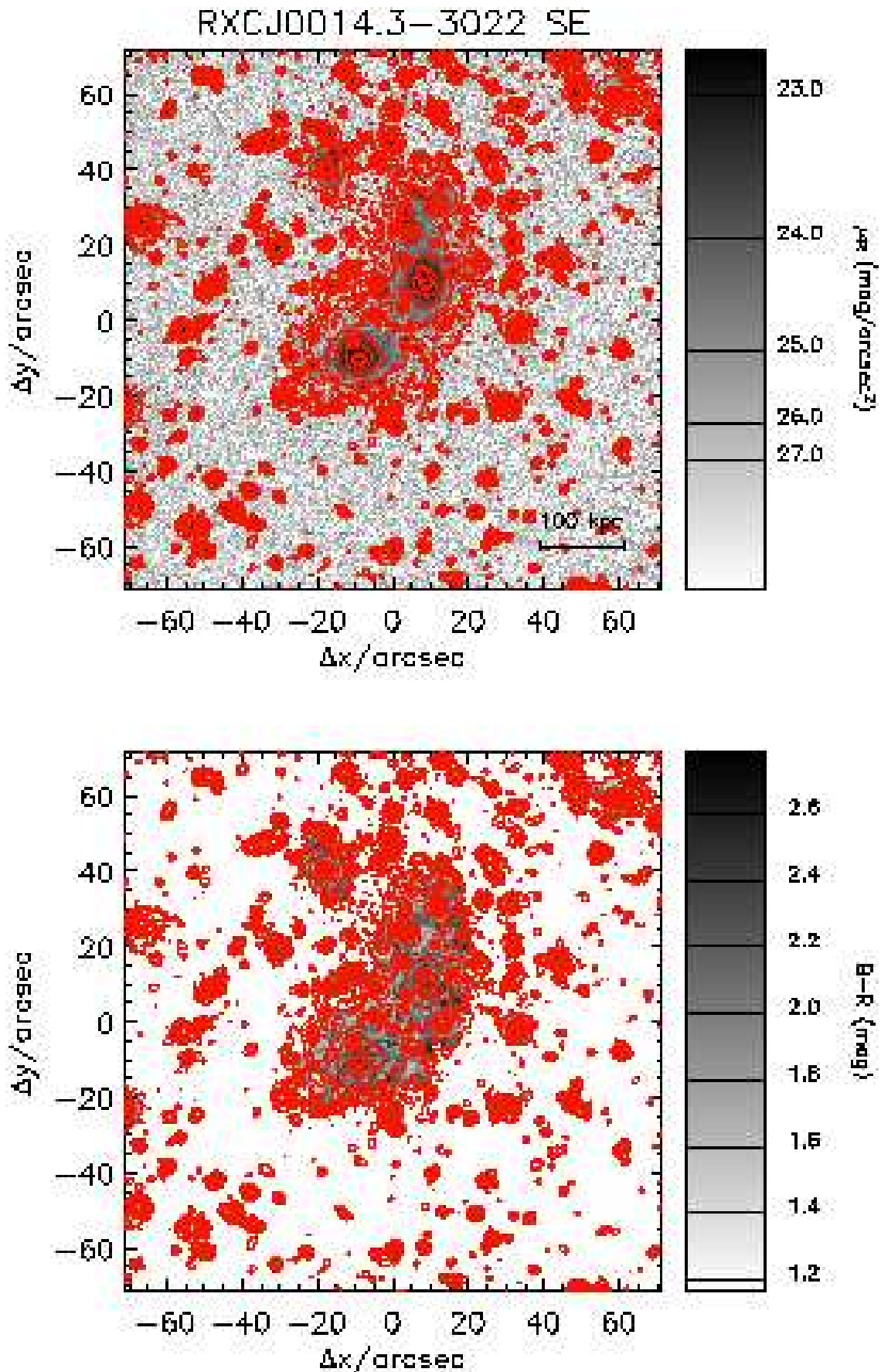


**Fig. 5.** The same as in Fig. 4 but for the SE pair of BCGs in RXCJ 0014.3-3022. Bright galaxies as red as the BCGs are at  $z \sim 0.3$  (Braglia et al. 2007).

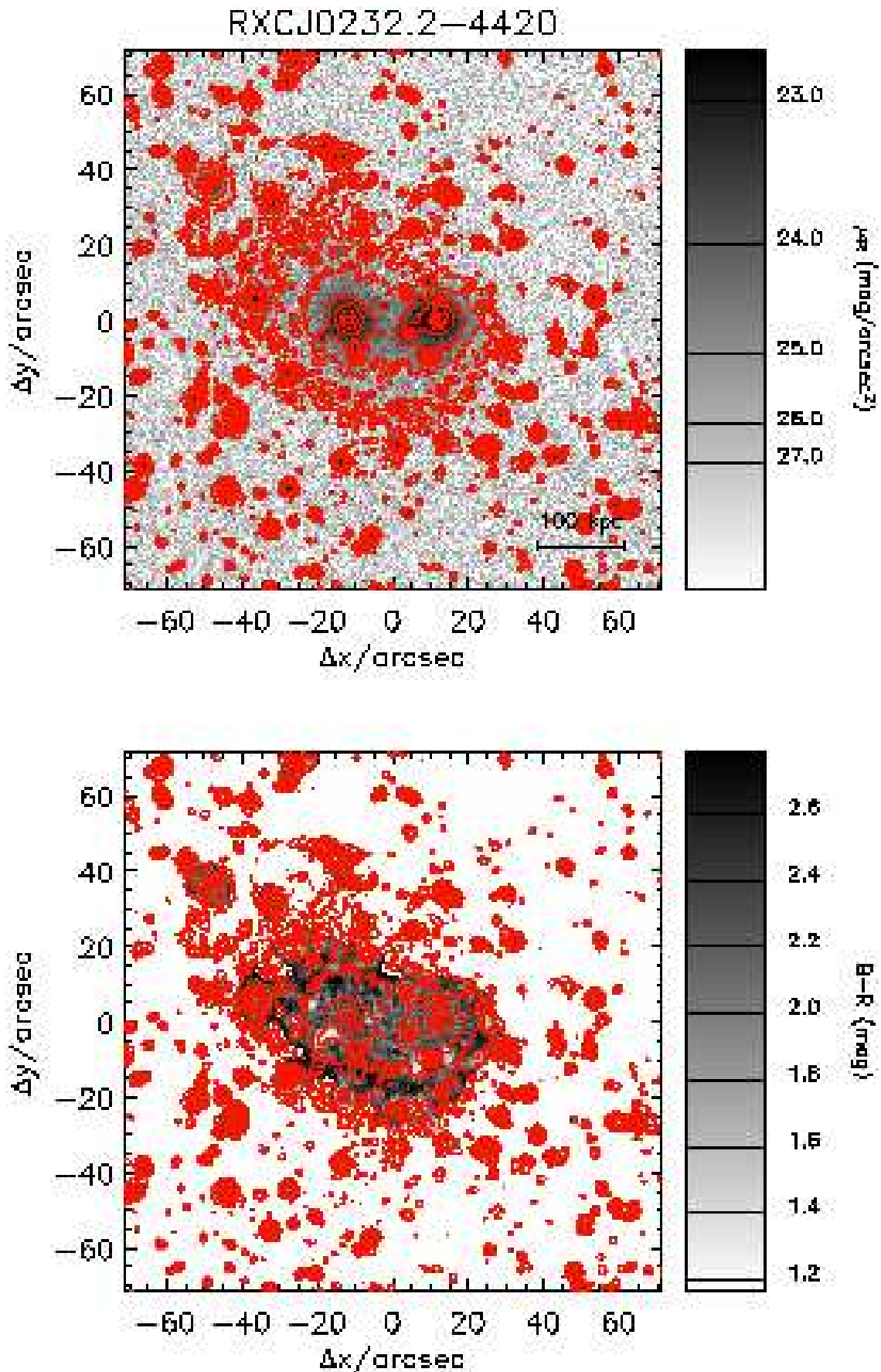


**Fig. 6.** The same as in Fig. 4 but for the pair of BCGs in RXCJ 0232.2-4420. Bright galaxies as red as the BCGs are likely at  $z \sim 0.3$ , as confirmed for RXCJ 0014.3-3022 (Braglia et al. 2007).

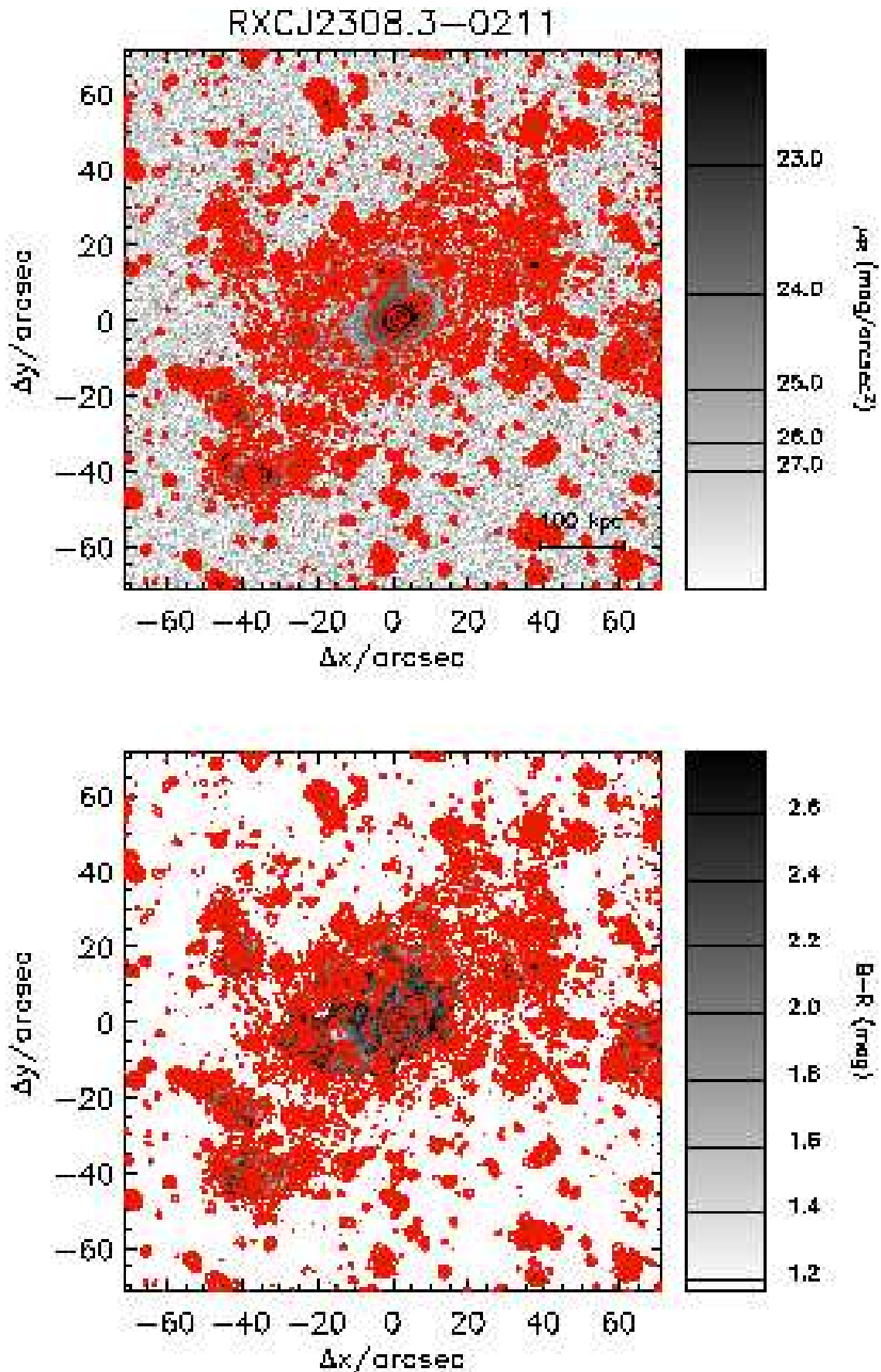


**Fig. 7.** The same as in Fig. 4 but for the single BCG in RXCJ 2308.3-0211. Bright galaxies as red as the BCG are likely at  $z \sim 0.3$ , as confirmed for RXCJ 0014.3-3022 (Braglia et al. 2007).



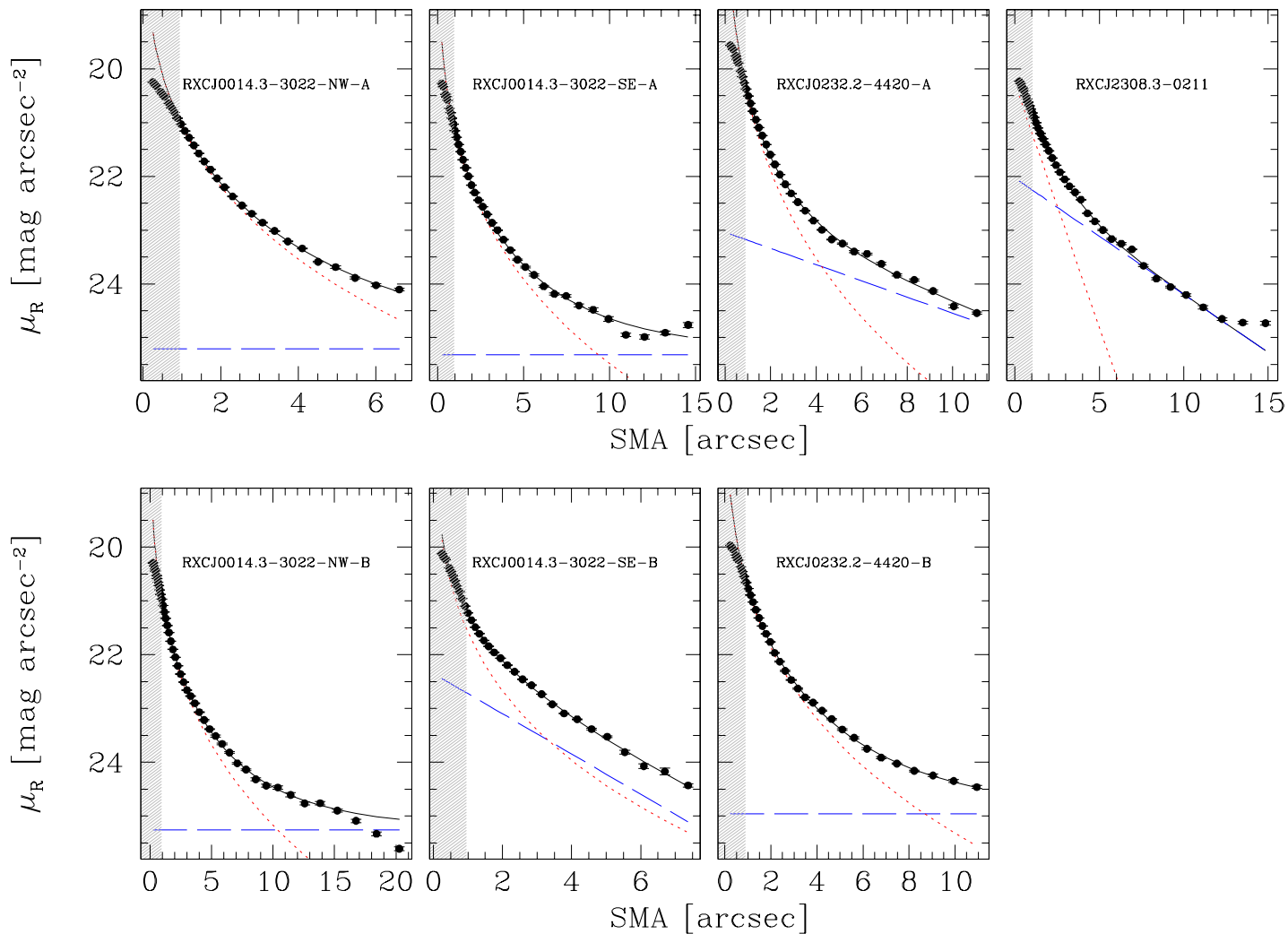


**Fig. 8.** R-band radial surface brightness profiles of the BCGs. In each panel, inner “de Vaucouleurs” (except for the BCG in RXCJ 2308.3–0211) and outer exponential components are marked with dotted and long-dashed lines, respectively, whereas a solid line represents the total best-fit model. A grey shaded area marks the innermost region not used for the surface brightness profile fitting because affected by seeing. “SMA” stands for semi-major axis of the individual elliptical annuli (see text).

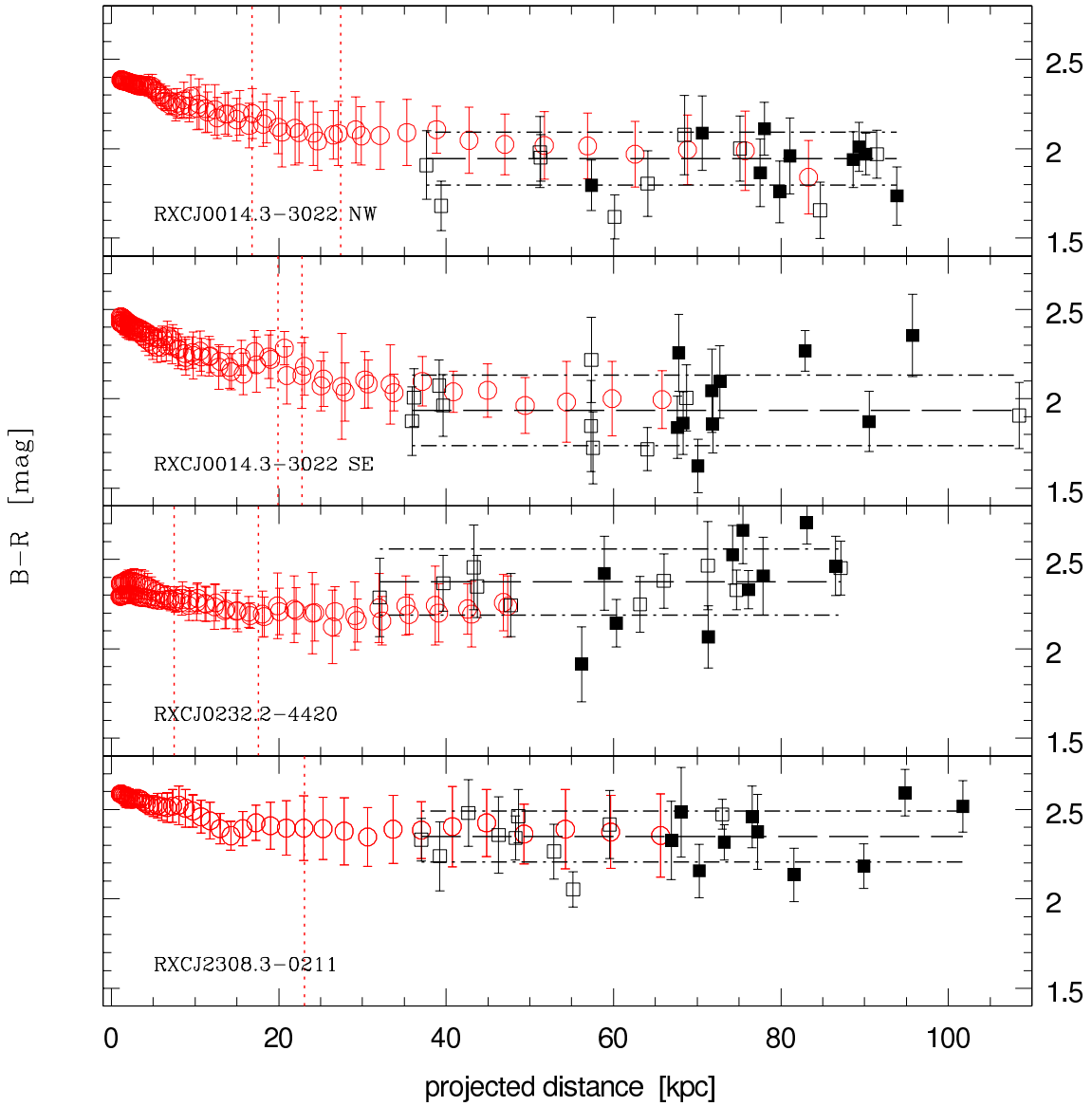


**Fig. 9.**  $B - R$  colours (observed frame) as measured at different projected radial distance from the centre of the (closest) BCG for the three pairs of BCGs RXCJ 0014.3-3022NW, RXCJ 0014.3-3022SE, RXCJ 0232.2-4420 plus the single BCG in RXCJ 2308.3-0211 listed in Table 2. In each panel, empty circles reproduce the radial  $B - R$  colour profile of each BCG measured in elliptical annuli; the RMS of the colour in each annulus is shown as an error bar. A vertical dotted line indicates the R-band effective radius of the BCG. Empty squares represent median values of the diffuse light estimated in 10 different 81 square pixel-regions (i.e., areas of  $\sim 90 \text{ kpc}^2$  at  $z = 0.3$ ) that are free from high-surface brightness emission associated with non-BCG galaxies and located all around each (pair of) BCG(s) but close to the 26 R-mag arcsec<sup>-2</sup> isophote. Filled squares represent median values of the diffuse light estimated in 10 different 81 square pixel-regions that are free from high-surface brightness emission associated with non-BCG galaxies and located at a projected distance of more than 50 kpc from any BCG. Error bars represent values of the standard deviation of the  $B - R$  colour distribution as probed in individual regions of the colour maps. Horizontal long-dashed and dot-dashed lines mark, respectively, the median and the median  $\pm 1$  RMS values of the colour of the diffuse stellar emission (see text).

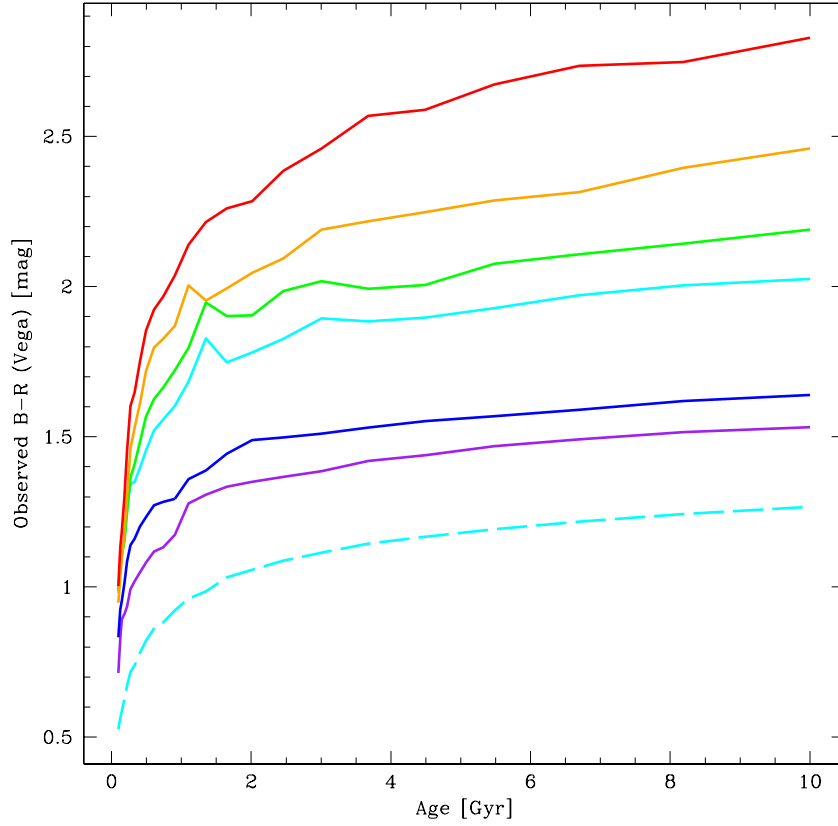


**Fig. 10.**  $B - R$  colours as a function of the epoch since star formation started (i.e., the “age”) and metallicity for models with different star-formation histories (Bruzual & Charlot 2003) redshifted to  $z = 0.3$ . From top to the bottom, solid curves reproduce simple stellar population models (i.e., models of a single burst of star formation) with fixed metallicity  $Z$  equal to  $2.5$ ,  $1$ ,  $0.4$ ,  $0.2$ ,  $0.02$ , and  $0.005 \times Z_{\odot}$ , respectively. The long-dashed curve reproduces models with constant star formation rate and  $Z = 0.2 \times Z_{\odot}$ . All models share the same stellar initial mass function (Chabrier 2003).

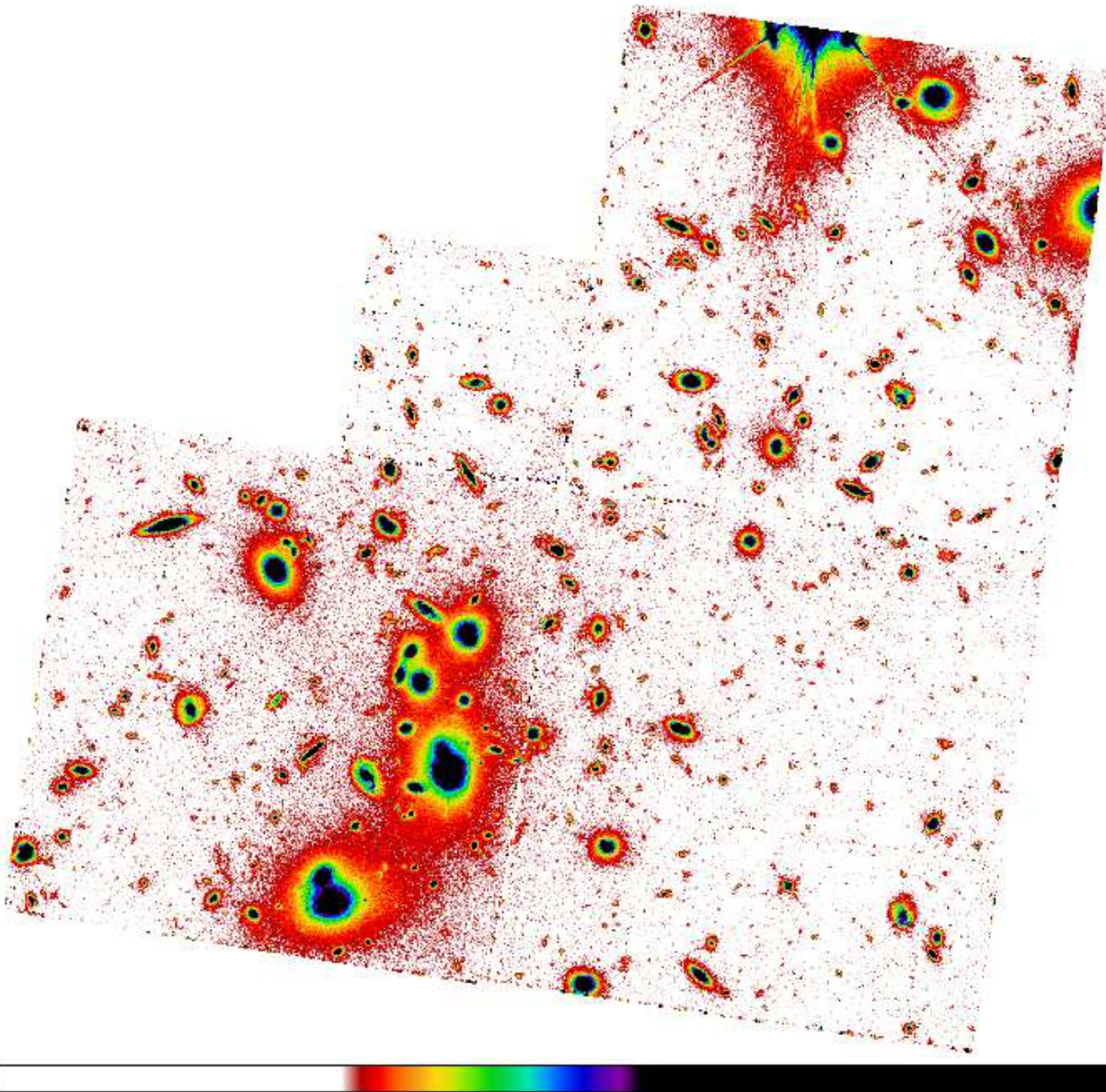


**Fig. 11.** Archival image of the RXCJ0014.3–3022 cluster core at a spatial resolution of  $0.3''$  (north is up and east to the left). It was obtained from a 36 min-exposure in the F702W filter - analogous to the R-band filter - with the Wide Field Planetary Camera (WFPC2) of the Hubble Space Telescope (HST) (see Couch et al. 1998). This reproduction highlights galaxy features at low surface brightness with a linear scale where intensity increases as the colour turns from white to black.